A microcavity-controlled, current-driven, on-chip nanotube emitter at infrared wavelengths

FENGNIAN XIA*, MATHIAS STEINER, YU-MING LIN AND PHAEDON AVOURIS*

Department of Nanometer Scale Science and Technology, IBM Thomas J. Watson Research Center, 1101 Kitchawan Rd, PO Box 218, Yorktown Heights, New York 10598, USA

***e-mail: fxia@us.ibm.com; avouris@us.ibm.com**

Published online: 24 August 2008; doi:10.1038/nnano.2008.241

Recent studies of the optical properties of semiconducting single-walled carbon nanotubes[1–6] suggest that these truly nanometre-scale systems have a promising future in nanophotonics, in addition to their well-known potential in electronics[7,8]. Semiconducting single-walled nanotubes have a direct, diameter-dependent bandgap[8] and can be excited readily by current injection, which makes them attractive as nano-emitters. The electroluminescence is spectrally broad, spatially non-directional, and the radiative yield is low[5,9]. Here we report the monolithic integration of a single, electrically excited, semiconducting nanotube transistor with a planar $\lambda/2$ microcavity[10–13], thus taking an important first step in the development of nanotube-based nanophotonic devices. The spectral full-width at half-maximum of the emission is reduced from ~300 to ~40 nm at a cavity resonance of 1.75 μm, and the emission becomes highly directional. The maximum enhancement of the radiative rate is estimated to be 4. We also show that both the optically and electrically excited luminescence of single-walled nanotubes involve the same E_{11} excitonic transition.

Successful application of individual, electrically driven emitters in nanophotonics, quantum optics or quantum communications, which has been demonstrated with individual quantum dots[14], has not been reported so far for single-walled carbon nanotubes. Embedding spatially isolated nanotubes into an optical microcavity is a promising means of controlling and improving their radiative properties[15–17]. The control of these properties of nanotubes, especially in current-driven nanotubes, including emission wavelength, spectral width, emission direction and radiative yield through optical confinement, can result in their use in integrated nanophotonic circuits[18].

The device reported here integrates a back-gated, light-emitting field effect transistor (FET) based on a single semiconducting single-walled nanotube[19,20] with a planar optical $\lambda/2$ microcavity[10–13]. A three-dimensional schematic view of the structure is shown in Fig. 1a. The photonic microcavity consists of three dielectric layer stacks: 250 nm of polymethyl methacrylate (PMMA), 22 nm of aluminium oxide (Al_2O_3) deposited using atomic layer deposition, and 250 nm of silicon oxide (SiO_2) sandwiched between a top gold mirror (20 nm) and a parallel bottom silver mirror (100 nm). An individual nanotube is placed on top of the Al_2O_3 layer close to the microcavity centre and is orientated parallel to the silver and the gold mirrors to provide optimum coupling conditions between the nanotube and the available photonic

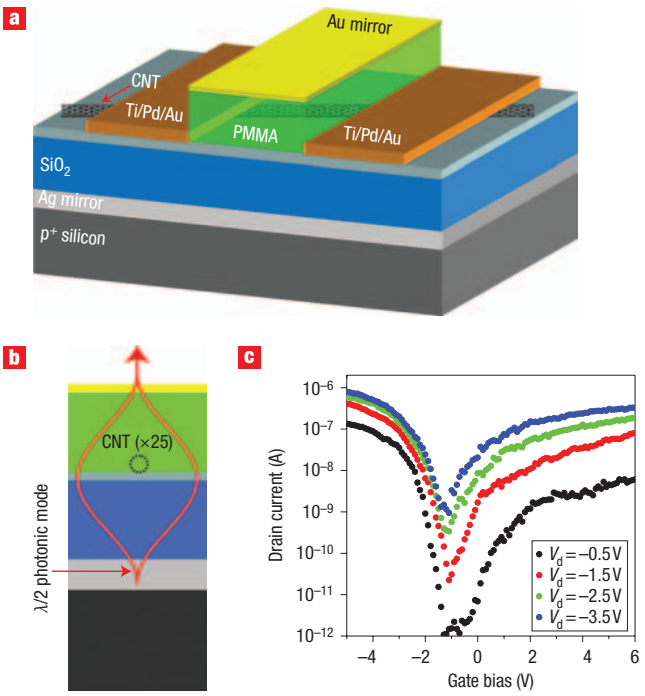

Figure 1 Schematic view of the integrated device and its electronic properties. a, 3D schematic representation of the microcavity-controlled infrared nano-light source comprising an FET integrated with a planar $\lambda/2$ microcavity. The source and drain electrodes made from Ti/Pd/Au (1/20/20 nm) are separated by 2 μm. **b**, Schematic $\lambda/2$ photonic mode profile showing the geometrical overlap of the nanotube and the spatial intensity distribution. The microcavity is formed by the Au and Ag mirrors and the light is emitted through the top Au mirror. The red arrow shows the emission direction of the on-axis mode. **c**, Typical electrical transport characteristics (drain current versus gate bias) at four different drain voltages.

© 2008 Macmillan Publishers Limited. All rights reserved.

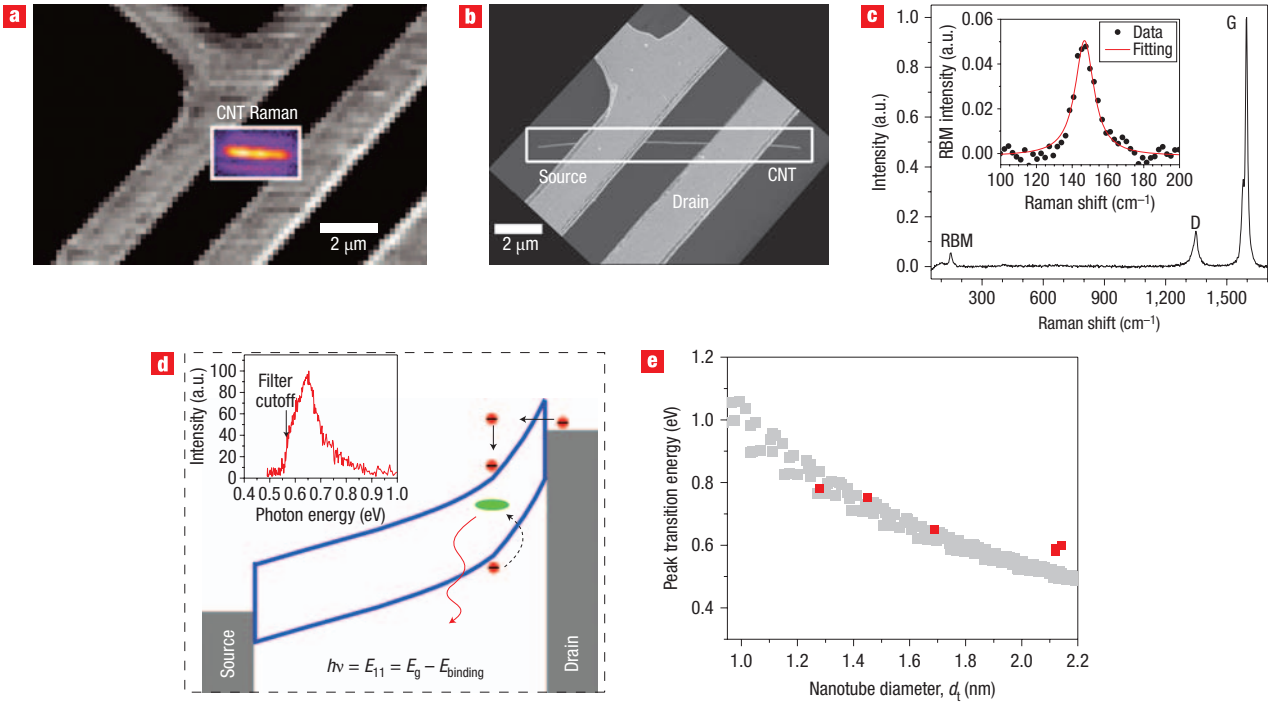

Figure 2 Carbon nanotube characterization and emission mechanism identification. a, Elastic scattering image of a CNT-FET taken without PMMA and top gold mirror. Inset: Raman scattering (G-band) intensity image of an isolated nanotube. **b**, Scanning electron micrograph of the same device. **c**, Raman spectrum measured for the same nanotube. Inset: Raman band associated with the RBM. **d**, Band diagram of an electrically driven nanotube emitter under a high-bias condition. The green oval denotes an excitonic state. Inset: electrically excited emission spectrum of a nanotube from which the Raman spectrum in **c** was taken. **e**, Emission peak energy (E_{peak}) versus nanotube diameter (d_t) plot. Solid red squares: experimental values obtained in this experiment. For individual nanotubes, the peak energies were obtained from the electroluminescence spectra and d_t was derived from the RBM frequency Ω_{RBM} in the corresponding Raman spectra using $d_t = 248/\Omega_{RBM}$ (ref. 23). Solid grey squares: empirical $d_t \sim E_{11}$ Kataura plot adapted from ref. (26).

microcavity modes[13]. The top gold mirror is a partial reflection mirror that allows for the out-coupling of the cavity mode. A schematic on-axis cavity mode intensity profile is shown in Fig. 1b.

Integration of a three-terminal FET with an optical cavity provides a significant challenge because of simultaneous, stringent electrical and optical requirements. The bottom silver mirror and the 250 nm silicon oxide (SiO_2) layer were deposited using e-beam evaporation. However, gating through e-beam-deposited SiO_2 can lead to high gate leakage, and the rough e-beam oxide surface can prevent close contact of the nanotube with the surface. Deposition of an additional 22-nm, high-quality Al_2O_3 layer using atomic layer deposition at a low temperature (200 °C) not only reduces the root-mean-square roughness of SiO_2 from 3.5 to 1.3 nm because of the conformal nature of the deposition, but also significantly improves the overall quality of the gate's dielectric stacks. Moreover, the low-temperature atomic layer deposition keeps the silver mirror intact. The electrical transport characteristics (that is, drain current versus gate bias) at different drain voltages for a representative single carbon nanotube (CNT)-FET are shown in Fig. 1c. Unlike a conventional silicon-based transistor that shows unipolar transport characteristics, the CNT-FET works as a Schottky-barrier-type FET exhibiting ambipolar behaviour[21,22]. Detailed information about the fabrication and optical properties of the device is presented in the Methods.

To identify the origin of the electroluminescence of the nanotube, both Raman and free-space electroluminescence spectra from nanotube devices were measured without the top gold mirror. As a result, the effect of optical confinement is negligible and the emission properties are determined by the intrinsic properties of the nanotube. In Fig. 2a, the centre of the elastic light-scattering image of a CNT-FET is overlapped with an image of the integrated Raman G-band intensity measured from an isolated nanotube. A scanning electron micrograph from the same device is shown in Fig. 2b. A Raman spectrum of the same nanotube is plotted in Fig. 2c, exhibiting the well-known scattering peaks associated with Raman-active phonon modes—that is, the radial breathing mode (RBM)—the disorder-induced phonon mode (D) and the main tangential G-band[23]. From the measured centre frequency of the RBM, $\Omega_{RBM} = 145\ cm^{-1}$ (see inset of Fig. 2c), the diameter of this specific nanotube is determined to be 1.7 nm using $d_t = 248/\Omega_{RBM}$ (ref. 23), a relation commonly used to find the diameter of the nanotube in the range $1\ nm < d_t < 2\ nm$. The corresponding electroluminescence spectrum measured for the same nanotube is shown in the inset of Fig. 2d, exhibiting a maximum at 0.65 eV and a spectral width of ~100 meV. Details about Raman and emission spectrum measurements are presented in the Methods. For the emission measurements, the source and gate electrodes of the CNT-FET were grounded and the drain electrode of the FET was biased at −10 V. The resulting drain current typically ranged between 5 and 10 μA. A schematic representation of a nanotube band profile under such biasing conditions is shown in Fig. 2d. Here, electrons are the main carrier injected from the drain, accumulating kinetic energy in

© 2008 Macmillan Publishers Limited. All rights reserved.

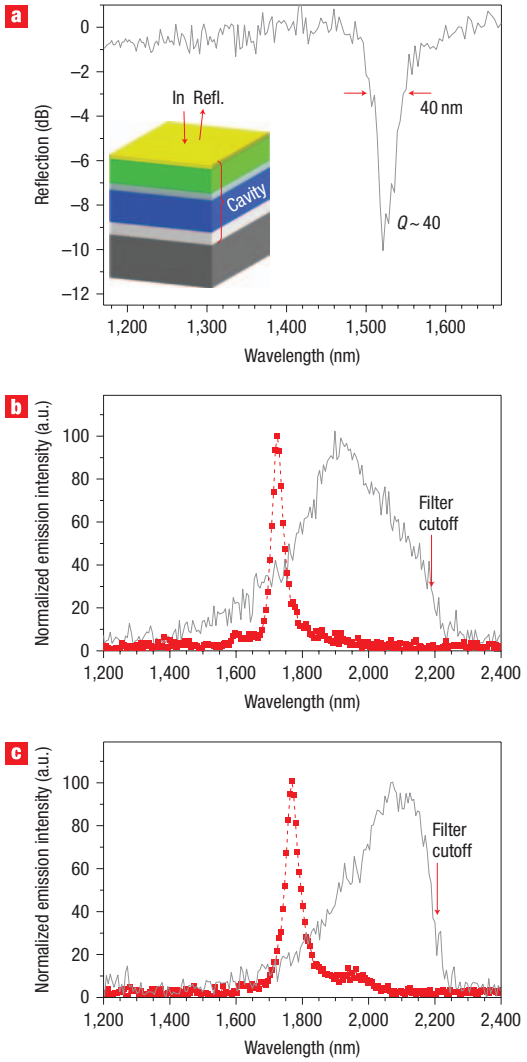

Figure 3 Microcavity-controlled electroluminescence spectra of carbon nanotubes. a, The reflection spectrum of the optical $\lambda/2$ microcavity measured near normal incidence from a reference sample showing a cavity quality (Q) factor of 40. Inset: schematic of the photonic microcavity. **b**,**c**, Electroluminescence spectra from two different nanotube devices with (dashed red) and without (solid grey) top gold cavity mirrors under electrical excitation ($V_s = V_g = 0$ V; $V_d \sim -10$ V). All spectra were collected using a microscope objective lens with an NA of 0.26. The wide emission spectra peaking at 1,900 (**b**) and 2,100 nm (**c**), respectively, are both transformed into narrow, cavity-controlled emission spectra peaking ~1,750 nm.

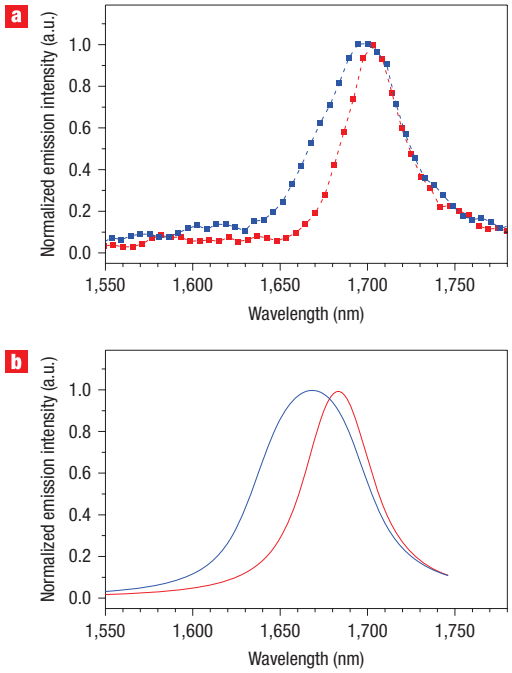

Figure 4 Angle dependence of the microcavity-controlled emission. Comparison of the measured (**a**) and calculated (**b**) microcavity-controlled electroluminescence spectra from the same carbon nanotube for a collection angle of 10° and NA = 0.26 (red lines) and an angle of 15° and NA = 0.4 (blue lines).

the high-field region near the Schottky barrier to generate excited states by means of impact excitation[5,9,24,25], a process whose efficiency is greatly enhanced in a one-dimensional nanotube compared with that in bulk solids. The radiative decay of these excitons leads to light emission. This localized excitonic emission process is different from those previously demonstrated[3,4] in which the nanotubes were biased such that both electrons and holes were injected simultaneously and their radiative recombination generated light.

In Fig. 2e, the measured peak energies of the free-space electroluminescence spectra are plotted against the tube diameter d_t as derived from the Raman measurements. Also plotted in Fig. 2e are the energies of the lowest-lying dipole-active excitonic transition, the so-called E_{11} transition, as a function of the nanotube diameter obtained by photoluminescence excitation spectroscopy (Kataura plot)[26]. A good agreement is obtained between our results and that from the Kataura plot for diameters below 1.7 nm, proving that electroluminescence from nanotubes involves the same E_{11} excitonic transition as observed in the photoluminescence of nanotubes in suspension. Although excitonic peaks do shift (20–50 meV) as a function of the dielectric environment, there is little difference in the effective dielectric constants for a nanotube on SiO_2 (half-space, $\varepsilon_{eff} \approx 2.5$), embedded in PMMA ($\varepsilon_{eff} \approx 2.6$–$3$) or suspended in solution ($\varepsilon_{eff} \approx 3$). This enables us to compare our results with that of a Kataura plot based on solution data. The relatively wide electroluminescence spectrum (~100 meV), compared with the photoluminescence spectrum[1,27] (~25 meV), is probably because of the high exciton density produced electrically and the subsequent fast exciton–exciton annihilation[5].

A similar reference $\lambda/2$ cavity sample with the same metallic and dielectric layer stacks but with a slightly smaller mirror spacing without electrodes and nanotubes was fabricated as shown in the inset of Fig. 3a. A representative reflection spectrum measured near normal incidence is plotted in Fig. 3a to reveal the on-axis resonance at 1,520 nm. From the spectral full-width at half-maximum (FWHM) of 40 nm, we derive an experimental cavity quality (Q) factor, $Q = \lambda/\Delta\lambda = 40$. We again measured the electroluminescence spectra of all devices after deposition of the gold top mirror (see Fig. 1a). In Fig. 3b,c, the free-space electroluminescence spectra of two different nanotubes (solid grey) are compared with the respective microcavity-controlled electroluminescence spectra (dashed red) measured under similar biasing conditions as mentioned above. The key observation is a strong spectral narrowing of the free-space emission of individual

© 2008 Macmillan Publishers Limited. All rights reserved.

nanotubes matching the spectral position, line shape and line width of the longitudinal photonic (forward) mode of the microcavity. Regardless of the specific structure of individual nanotubes, their free-space emissions with line widths of 300 nm were spectrally redistributed to produce a narrow, almost symmetric spectrum with an FWHM of ~40 nm, 13% of the original value. The slight differences in peak emission wavelengths for the cavity-controlled spectra of the two different devices in Fig. 3b and c are caused by small non-uniformities in optical layer thickness.

To demonstrate the spectral-angle redistribution of the electroluminescence, we also measured and simulated the correlation between the collection angle and the spectral distribution using two different objective lenses having numerical apertures (NAs) of 0.26 and 0.40, which provide collection angles (θ) of 10° and 15°, respectively (see Supplementary Information, inset of Fig. S1). Further information about the simulation including the radiative rate modifications is given in Supplementary Information. Two microcavity-controlled experimental spectra from the same nanotube, but collected using two different objectives are plotted, respectively, as red and blue dashed curves in Fig. 4a, and the corresponding calculated spectra are shown in Fig. 4b. The increase in the spectral width with increasing NA is a consequence of the increased detection efficiency for off-axis emissions. Small differences in peak positions of the spectra shown in Fig. 4a and b are caused by slight deviations of the dielectric layer thicknesses with respect to their nominal values used in the calculations.

Integration of current-driven nanotubes with silicon nanocavities having a high quality factor and small mode volume[28] may ultimately lead to low threshold on-chip nanolasers[29]. However, exciton–exciton annihilation[5] may set an upper limit for the exciton density achievable in carbon nanotubes. Saturation of nanotube photoluminescence[30] under intense optical excitation has also been observed and attributed to this annihilation process. Whether such an annihilation process would prevent population inversion and lasing from being achieved remains an open question in the nanotube community and needs further investigation.

In summary, we reported the first on-chip integration of an optical $\lambda/2$ microcavity and an FET based on a semiconducting single-walled nanotube forming a current-driven, highly directed and spectrally narrow infrared nano-light source. Such nano-light sources may find applications in integrated nanophotonic circuits, quantum optics and on-chip optical interconnects.

METHODS

FABRICATION OF THE MICROCAVITY-CONTROLLED NANO-LIGHT SOURCE BASED ON A CNT-FET

Fabrication of the device began with the deposition of a 100-nm silver layer and a 250-nm silicon oxide (SiO_2) layer on a p^+ silicon substrate using e-beam evaporation. The 250-nm silicon oxide is the dielectric material at the bottom-half of the planar photonic $\lambda/2$ cavity. A 22-nm Al_2O_3 layer was then deposited on top of the SiO_2 using the atomic layer deposition method. The nanotubes produced by arc-discharge were then dispersed on the wafer, and blank photolithography was used to pattern the source and drain areas. Ti/Pd/Au (1/20/20 nm) films were deposited using e-beam evaporation and, following lift-off, formed the source and drain contacts. A layer of 250-nm PMMA was then spin-coated to serve as the top-half dielectric material of the photonic $\lambda/2$ microcavity. PMMA in selected areas was exposed using e-beam lithography and removed so that the source and drain metal pads could be probed using probing needles. Finally, a thin layer of gold (~20 nm) was deposited as the upper microcavity mirror using e-beam evaporation with a shadow mask to avoid shorting of the source and drain contacts. The 20-nm thick gold mirror on top effectively forms the out-coupling mirror of the optical cavity. For typical electroluminescence wavelengths between 1,500 and 2,000 nm, the gold mirror has a reflectivity of ~92% and a transmittance of ~5% using $n_{Au} = 0.7 + 11i$ at normal incidence. The reflectivity of the bottom silver mirror with a thickness of 100 nm is 97% for near-infrared radiation using $n_{Ag} = 0.8 + 12i$ at normal incidence, and the transmission through 100 nm of silver is negligible. Fabrication of the separate, reference cavity sample is similar to the above process flow, except that the nanotubes and contact pads are not involved. The cavity resonance of the reference cavity sample is intentionally designed to be below 1,600 nm (by modifying the dielectric layer thickness), because this is the longest wavelength our cavity characterization setup (fibre-generated 'continuum' source) can access.

MEASUREMENT OF THE RAMAN SPECTRA OF CARBON NANOTUBES

Raman images and spectra were acquired using a scanning optical microscope equipped with a standard microscope objective (×100, NA = 0.9), providing a focal spot diameter of ~0.5 μm and a power density of ~250 kW cm^{-2}. The excitation light (from an argon-ion laser operated at 514.5 nm or a He–Ne laser operated at 632.8 nm) was focused directly on individual nanotubes without the upper cavity mirror and the PMMA layer (see Fig. 1a) and scanned along the device. The Raman scattering intensity was recorded at the location of the excitation spot. Raster scanning the device with respect to the microscope objective was accomplished by a feedback-controlled, piezoelectric scanning stage. The Raman-scattered light was separated from the laser excitation light using holographic notch filters and detected by a spectrograph with a grating that had a groove density of 1,200 mm^{-1} and a liquid-nitrogen-cooled charge-coupled device detector, resulting in a spectral resolution of 2 cm^{-1}. Spatially localized and identified individual nanotubes were positioned at the focal spot of the microscope objective, and Raman spectra having sufficient signal-to-noise ratios were acquired with integration times ranging between 90 and 300 s to clearly reveal RBM signatures (see Fig. 2c). To improve the data quality, a corresponding background spectrum measured with the same set of acquisition parameters was subtracted from each measured Raman spectrum.

MEASUREMENT OF THE ELECTROLUMINESCENCE SPECTRA OF NANOTUBES

The light emitted by an individual nanotube is collected using microscope objectives with different NAs (0.26 or 0.4 in our experiments), filtered by an optical band-pass filter having a transmission window between 1,400 and 2,215 nm, spectrally dispersed using a grism (an optical device combining a prism and a grating) and finally detected using a liquid-nitrogen-cooled HgCdTe detector array of 256 × 256 pixels. The spectral resolution per pixel is 5.5 nm. The spatial distribution of the nanotube emission cannot be determined using conventional far-field optics here, because the length of the nanotube (~2 μm) is comparable with the emission wavelength.

Received 29 February 2008; accepted 24 July 2008; published 24 August 2008.

References

1. O'Connell, M. J. *et al.* Bandgap fluorescence from individual single-walled carbon nanotubes. *Science* **297,** 593–596 (2002).
2. Bachilo, S. M. *et al.* Structure-assigned optical spectra of single-walled carbon nanotubes. *Science* **298,** 2361–2366 (2002).
3. Misewich, J. A. *et al.* Electrically induced optical emission from a carbon nanotube FET. *Science* **300,** 783–786 (2003).
4. Freitag, M. *et al.* Mobile ambipolar domain in carbon-nanotube infrared emitters. *Phys. Rev. Lett.* **93,** 076803 (2004).
5. Chen, J. *et al.* Bright infrared emission from electrically induced excitons in carbon nanotubes. *Science* **310,** 1171–1174 (2005).
6. Freitag, M., Martin, Y., Misewich, J. A., Martel, R. & Avouris, P. Photoconductivity of single carbon nanotubes. *Nano Lett.* **3,** 1067–1071 (2003).
7. Avouris, P., Chen, Z. & Perebeinos, V. Carbon-based electronics. *Nature Nanotech.* **2,** 605–615 (2007).
8. Biercuk, M. J., Ilani, S., Marcus, C. M. & McEuen, P. L. in *Carbon Nanotubes: Advanced Topics in the Synthesis, Structure, Properties and Applications* (eds Jorio, A., Dresselhaus, M. S. & Dresselhaus, G.) (Springer, Berlin, 2008).
9. Marty, L. *et al.* Exciton formation and annihilation during 1D impact excitation of carbon nanotubes. *Phys. Rev. Lett.* **96,** 136803 (2006).
10. Brorson, S. D., Yokoyama, H. & Ippen, E. Spontaneous emission rate alteration in optical waveguide structures. *IEEE J. Quantum Electron.* **26,** 1492–1499 (1990).
11. Yamamoto, Y., Machida, S. & Bjork, G. Micro-cavity semiconductor lasers with controlled spontaneous emission. *Opt. Quantum Electron.* **24,** S215–S243 (1992).
12. Björk, G. On the spontaneous lifetime change in an ideal planar microcavity-transition from a mode continuum to quantized modes. *IEEE J. Quantum Electron.* **30,** 2314–2318 (1994).
13. Abram, I., Robert, I. & Kuszelewicz, R. Spontaneous emission control in semiconductor microcavities with metallic or Bragg mirrors. *IEEE J. Quantum Electron.* **34,** 71–76 (1998).
14. Yuan, Z. *et al.* Electrically driven single-photon source. *Science* **295,** 102–105 (2002).
15. Steiner, M., Qian, H., Hartschuh, A. & Meixner, A. J. Controlling non-equilibrium phonon populations in single-walled carbon nanotubes. *Nano Lett.* **8,** 2239–2242 (2007).
16. Vahala, K. J. Optical microcavities. *Nature* **424,** 839–846 (2003).
17. Steiner, M. *et al.* Microcavity-controlled single-molecule fluorescence. *ChemPhysChem* **6,** 2190–2196 (2005).
18. Xia, F., Sekaric, L. & Vlasov, Y. A. Ultra-compact optical buffers on a silicon chip. *Nature Photon.* **1,** 65–71 (2007).
19. Tans, S. J., Verscheuren, A. R. M. & Dekker, C. Room-temperature transistor based on a single carbon nanotube. *Nature* **393,** 49–52 (1998).
20. Martel, R., Schmidt, T., Shea, H. R., Hertel, T. & Avouris, P. Single- and multi-wall carbon nanotube field-effect transistors. *Appl. Phys. Lett.* **73,** 2447–2449 (1998).

© 2008 Macmillan Publishers Limited. All rights reserved.

21. Martel, R. *et al*. Ambipolar electrical transport in semiconducting single-wall carbon nanotubes. *Phys. Rev. Lett.* **87,** 256805 (2001).
22. Heinze, S. *et al*. Carbon nanotubes as Schottky barrier transistors. *Phys. Rev. Lett.* **89,** 106801 (2002).
23. Dresselhaus, M. S., Dresselhaus, G., Saito, R. & Jorio, A. Raman spectroscopy of carbon nanotubes. *Phys. Rep.* **409,** 47–99 (2005).
24. Perebeinos, V. & Avouris, P. Impact excitation by hot carriers in carbon nanotubes. *Phys. Rev. B* **74,** 121410R (2006).
25. McGuire, D. L. & Pulfrey, D. L. A multi-scale model for mobile and localized electroluminescence in carbon nanotube field-effect transistors. *Nanotechnology* **17,** 5805–5811 (2006).
26. Weisman, R. B. & Bachilo, S. M. Dependence of optical transition energies on structure for single-walled carbon nanotubes in aqueous suspension: an empirical Kataura plot. *Nano Lett.* **3,** 1235–1238 (2003).
27. Lefebvre, J., Austing, D. G., Bond, J. & Finnie, P. Photoluminescence imaging of suspended single-walled carbon nanotubes. *Nano Lett.* **6,** 1603–1608 (2006).
28. Song, B. S., Noda, S., Asano, T. & Akahane, Y. Ultra-high-*Q* photonic double-heterostructure nanocavity. *Nature Mater.* **4,** 207–210 (2005).
29. Noda, S. Seeking the ultimate nanolaser. *Science* **314,** 260–261 (2006).
30. Murakami, Y. & Kono, J. Nonlinear photoluminescence excitation spectroscopy of carbon nanotubes: exploring the upper density limit of one-dimensional excitons. Preprint at http://arxiv.org/abs/0804.3190 (2008).

Supplementary Information accompanies this paper at www.nature.com/naturenanotechnology.

Acknowledgements

The authors thank M. Freitag, Z. Chen, Yu. A. Vlasov, S. Assefa and W. G. Green for helpful discussions, J. Tsang and M. Kinoshita for help with the emission spectra measurements, J. Small for help with the cavity *Q* measurement, B. Ek for technical support and Central Scientific Services in IBM Thomas J. Watson Research Center for metal deposition and mask fabrications.

Author information

Reprints and permission information is available online at http://npg.nature.com/reprintsandpermissions/. Correspondence and requests for materials should be addressed to F.X. and P.A.

© 2008 Macmillan Publishers Limited. All rights reserved.